A-site doping-induced renormalization of structural transformations in the $PbSc_{0.5}Nb_{0.5}O_3$ relaxor ferroelectric under high pressure

B. J. Maier,[1,*] A.-M. Welsch,[1] R. J. Angel,[2] B. Mihailova,[1,†] J. Zhao,[2] J. M. Engel,[3] L. A. Schmitt,[4] C. Paulmann,[1] M. Gospodinov,[5] A. Friedrich,[6] and U. Bismayer[1]

[1]*Department Geowissenschaften, Universität Hamburg, Grindelallee 48, D-20146 Hamburg, Germany*

[2]*Virginia Tech Crystallography Laboratory, Department of Geosciences, Virginia Tech, Blacksburg, Virginia 24060, USA*

[3]*Institut für Werkstoffwissenschaften, Technische Universität Dresden, Helmholtzstr. 7, D-01069 Dresden, Germany*

[4]*Materials Science Structure Research, Universität Darmstadt, Petersenstr. 23, D-64287 Darmstadt, Germany*

[5]*Institute of Solid State Physics, Bulgarian Academy of Sciences, Boulevard Tzarigradsko Chausse 72, 1784 Sofia, Bulgaria*

[6]*Institut für Geowissenschaften, Goethe-Universität, Altenhöferallee 1, D-60438 Frankfurt am Main, Germany*

(Received 6 November 2009; revised manuscript received 8 February 2010; published 21 May 2010)

The effect of *A*-site incorporated Ba^{2+} and Bi^{3+} on the pressure-driven structural transformations in Pb-based perovskite-type relaxor ferroelectrics has been studied with *in situ* x-ray diffraction and Raman scattering of $PbSc_{0.5}Nb_{0.5}O_3$, $Pb_{0.93}Ba_{0.07}Sc_{0.5}Nb_{0.5}O_3$, and $Pb_{0.98}Bi_{0.02}Sc_{0.51}Nb_{0.49}O_3$ in the range from ambient pressure to 9.8 GPa. The substitution of Ba^{2+} for Pb^{2+} represents the case in which *A*-site divalent cations with stereochemically active lone-pair electrons are replaced by isovalent cations with a larger ionic radius and no active lone pairs, leading to formation of strong local elastic fields. In contrast, substitution of Bi^{3+} for Pb^{2+} involves the replacement of divalent *A*-site cations with active lone-pair electrons by aliovalent cations with nearly the same ionic radius and active lone pairs so it induces local electric fields but not strong elastic fields. The two types of dopants have rather distinct effects on the changes in the atomic structure under pressure. The embedding of Ba^{2+} and associated elastic fields hinders the development of pressure-induced ferroic ordering and thus smears out the phase transition. The addition of Bi^{3+} enlarges the fraction of spatial regions with a pressure-induced ferroic distortion, resulting in a more pronounced phase transition of the average structure, i.e., the preserved lone-pair order and the absence of strong local elastic fields enhances the development of the ferroic phase at high pressure. For all compounds studied, the high-pressure structure exhibits glide-plane pseudosymmetry associated with a specific octahedral tilt configuration.

DOI: 10.1103/PhysRevB.81.174116 PACS number(s): 61.50.Ks, 61.72.Dd, 64.70.Nd, 77.84.Ek

I. INTRODUCTION

Relaxor ferroelectrics are materials with outstanding dielectric, electroelastic, and electro-optic properties related to their complex nanoscale structure.[1,2] Due to their superior performance, relaxors and related materials are of great technological importance, including memory devices.[3] Relaxors exhibit a broad frequency-dependent peak of the dielectric permittivity as a function of temperature, which is related to the complexity of their structure.[1,4] The characterization of the structural peculiarities of relaxors has been challenging the material science community since their first synthesis and although they have been a subject of extensive studies over the past decade, the structure-property relationship is still a matter of debate.[1,2,4,5] Thus further structural analyses on model compounds are required to identify the specific atomic arrangements in relaxors.

The relaxor structural state consists of nanometer-sized polar regions (PNRs) dispersed in a paraelectric matrix.[6] PNRs occur at temperatures well above the temperature of the dielectric permittivity maximum T_m and for canonical relaxors, no development of PNRs into normal ferroelectric domains takes place below T_m.[1,2] Above and near T_m, PNRs are dynamic in nature on the 10^{-4}–10^{-5} s time scale while at low temperatures, the dynamics of PNRs dramatically slows down.[7] It is widely believed that the presence of inhomogeneities in chemistry and/or the state of cation order are the reason for the suppression of long-range ferroelectric order.[8,9] In particular, for perovskite-type compounds with the general formula $A(B',B'')O_3$, the relaxor features are usually considered in the context of chemical 1:1 *B*-site order (CBO): alternating B' and B'' sites along the cubic ⟨100⟩ directions. Relaxor behavior is observed for materials, which on the long-range scale, have partial or complete disorder on the *B* site. However, *A*-site chemical disorder, including isovalent substitution, also enhances relaxor properties.[10,11] This indicates that the mechanism by which chemical variations induces relaxor behavior is not clear; either local charge imbalance or local elastic strains resulting from substitution disorder may be responsible. It is the aim of the work reported in this paper to resolve this issue for the case of *A*-site chemical disorder.

Complementary high-pressure (HP) structural analyses, in addition to temperature-dependent studies, are of particular importance in the field of relaxors because the mechanical load can slow down dynamic structural fluctuations and thus can better reveal energetically preferred noncubic atomic clusters that may be present at ambient conditions but which are not enhanced upon cooling. The coexistence of such noncubic species along with the polar clusters that evolve with lower temperatures might also be responsible for the unique relaxor properties. Based on the results from dielectric experiments up to 2.0 GPa showing a crossover from a normal- to relaxor-ferroelectric state,[12] it was suggested that pressure gradually decreases the correlation length between PNRs and, hence, at higher pressures the relaxor system should be

driven to a pure paraelectric cubic state. That would explain the suppression of the x-ray diffuse scattering arising from the PNRs at high pressures[13–17] but it is inconsistent with HP Raman scattering which clearly indicates noncubic symmetries.[15–19] Further, our combined x-ray diffraction (XRD) and Raman spectroscopic analysis of $PbSc_{0.5}Ta_{0.5}O_3$ (PST) (Ref. 17) unambiguously demonstrated a pressure-induced second-order phase transition at 2 GPa in which the symmetry of the average structure is reduced from cubic, involving enhanced distortion of the coordination of the Pb atoms by O atoms.

It was subsequently shown that the substitution of Ba^{2+} for Pb^{2+} in the canonical relaxor $Pb_{0.78}Ba_{0.22}Sc_{0.5}Ta_{0.5}O_3$ smears out the pressure-induced phase transition over a pressure range, even though the CBO regions are larger in the Ba-doped material than in the pure material.[20] This suggests that the smearing is due to the local structural distortions and associated local elastic fields in the vicinity of the Ba^{2+} ions. Further, stoichiometric, Ba- and Bi-doped $PbSc_{0.5}Nb_{0.5}O_3$ (PSN) crystals exhibit distinctive temperature-driven transformation processes, which essentially depend on the lone-pair orientation order in the perovskite *A*-site sublattice.[21] The replacement of Pb^{2+} ions having stereochemically active lone-pair electrons (LPEs) by isovalent cations with an isotropic outermost electron shell (Ba^{2+}) suppresses the development of temperature-induced long-range ferroelectric order whereas the replacement of Pb^{2+} by aliovalent cations with LPEs (Bi^{3+}) enlarges the fraction of ferroelectric domains at low temperatures. These results from *in situ* temperature-dependent experiments suggest that chemically induced local elastic strains play a more important role than local change imbalance in the formation of the relaxor state, although the charge imbalance is commonly considered as the necessary prerequisite for the suppression of ferroelectric long-range order upon cooling. The aim of this paper is to further analyze the factors governing the suppression of ferroic long-range order in relaxors by determining the effect of *A*-site substitution on the pressure-driven structural transformations. For this purpose, we performed *in situ* high-pressure XRD and Raman-scattering measurements on same single crystals of stoichiometric, Ba- and Bi-doped PSN that have been previously studied under varying temperature.[21] In this paper, we will provide evidence that local elastic strain fields associated with substitutional disorder play a dominant role in the development of the high-pressure structural state of these materials, a result consistent with the previous observation that local elastic strains dominate the low-temperature behavior of these same materials.

II. EXPERIMENTAL DETAILS

Optically and chemically homogeneous, cubic-shaped single crystals of PSN, $Pb_{0.93}Ba_{0.07}Sc_{0.5}Nb_{0.5}O_3$ (PSN-Ba), and $Pb_{0.98}Bi_{0.02}Sc_{0.51}Nb_{0.49}O_3$ (PSN-Bi) were synthesized by the high-temperature solution growth method.[21] The chemical composition was determined by electron microprobe analysis (Camebax microbeam SEM system), averaging over 100 spatial points.

Transmission electron microscopy (TEM) was applied to probe the size and abundance of chemically 1:1 *B*-site ordered nanoregions. Single-crystal {110} oriented cuts with a thickness of 100 μm were prepared for TEM experiments. The slices were polished down to approximately 10 μm thickness and glued on a molybdenum grid. Mounted samples were then Ar^+ ion milled. The specimens were slightly carbon coated to prevent charging under the incident electron beam. TEM experiments were carried out on a Philips CM20 supertwin microscope operating at 200 kV. The studies comprised selected area electron diffraction (SAED) combined with high-resolution (HR) TEM imaging.

HP experiments were performed on samples of an approximate size $100\times100\times50$ μm^3. In-house single-crystal HP XRD experiments on PSN, PSN-Ba, and PSN-Bi were conducted using diamond-anvil cells (DACs) of the ETH (Ref. 22) type. Quartz was used as an internal standard to determine pressures with a precision of 0.01 GPa, using the equation of state of quartz.[23] Unit-cell parameters were determined by the method of eight-position diffracted beam centering[24] with full profile fitting and subsequent least-squares fit on a Huber four-circle diffractometer.[25] Equations of state (EoSs) were fitted to the p-V data sets using the program EOSFIT.[25]

Synchrotron single-crystal XRD experiments on PSN, PSN-Ba, and PSN-Bi were conducted at the F1 beamline of HASYLAB/DESY with a radiation wavelength $\lambda=0.5000$ Å. Data were collected with a MarCCD 165 detector at a sample-to-detector distance of 80 mm, a stepwidth of 0.5° per frame and an exposure time of 120 s. The HP experiments were performed using DACs of ETH (Ref. 22) and Boehler-Almax[26] design. The ruby-line luminescence method was used to determine pressure.[27] The collected data images were evaluated with the Oxford Diffraction software CRYSALIS. A mixture of methanol and ethanol in the ratio of 4:1 was used as a pressure medium in both types of XRD experiments to preserve hydrostatic conditions up to 9.8 GPa.[28]

The HP Raman experiments were performed with a gas-membrane-driven easyLab Diacell® μScopeDAC-RT(G), using a methanol-ethanol-water mixture in the ratio 16:3:1 as a pressure-transmitting medium, which ensured hydrostatic conditions in the pressure range up to 10.5 GPa.[28] The pressure was determined by the ruby-line luminescence method. Raman spectra were measured with a Horiba Jobin-Yvon T64000 triple-grating spectrometer, using the Ar^+ laser line with $\lambda=514.5$ nm. Data were collected in backscattering geometry with an Olympus microscope and a 50× long-working distance objective. All spectra were corrected for the Bose-Einstein occupational factor and smoothed by the adjacent averaging method with a coefficient 3. The latter procedure did not affect the full widths at half maximum (FWHMs) of the measured Raman peaks. The peak positions, FWHMs and the integrated intensities were determined by fitting the spectrum profiles with Lorentzian functions. The repeatability of spectral features was verified by measuring several samples of each compound.

Measurements on decompression confirmed the reversibility of the pressure-induced structural changes observed by XRD and Raman scattering.

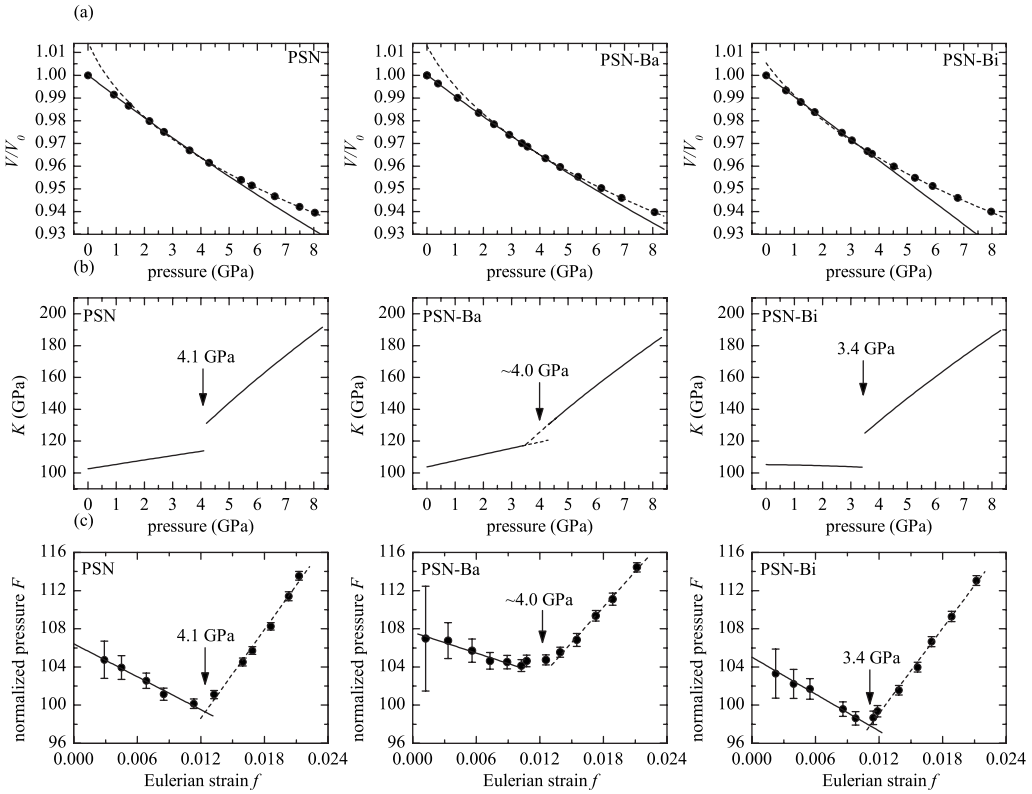

FIG. 1. Results of in-house single-crystal XRD experiments for PSN, PSN-Ba, and PSN-Bi: (a) pressure evolution of the volume, (b) pressure evolution of the bulk modulus obtained by the Birch-Murnaghan fits to the p-V data, and (c) f-F plots. The solid and dashed lines in (a) represent third-order Birch-Murnaghan fits below and above the phase transition, respectively. The arrows in (b) mark the phase-transition pressure. The EoS parameters fitted to the experimental points below p_c are $V_0=546.78\pm0.13$ Å^3, $K_0=103\pm3$ GPa, $K_0'=2.8\pm1.1$ for PSN, $V_0=546.42\pm0.14$ Å^3, $K_0=105\pm3$ GPa, $K_0'=3.5\pm1.6$ for PSN-Ba, and $V_0=544.57\pm0.08$ Å^3), $K_0=105\pm2$ GPa, $K_0'=-0.2\pm1.4$ for PSN-Bi.

III. RESULTS AND DISCUSSION

The pressure-induced evolution of the pseudocubic unit-cell volume of PSN, PSN-Ba, and PSN-Bi determined from in-house XRD experiments is shown in Fig. 1(a). All three compounds exhibit a change in the compressibility and consequently in the bulk modulus [see Fig. 1(b)]. Within the experimental accuracy of $\pm10^{-4}$ Å^3, no detectable discontinuity in the unit-cell volume was observed, which indicates that the pressure-induced phase transition is effectively thermodynamically contenuous.

The critical pressures and the character of the phase transitions are better revealed by the f-F plots [Fig. 1(c)], in which the normalized pressure $F=p/[3f(1+2f)^{5/2}]$ is plotted against the Eulerian finite strain $f=[(V_0/V)^{2/3}-1]/2$. The f-F plots of all three compounds clearly show elastic softening of both the low- and the high-pressure phase, as they approach the phase-transition point. For pure PSN, the critical pressure is near 4.1 GPa whereas the A-site doped compounds undergo a phase transition at slightly lower pressures, near 4.0 GPa for PSN-Ba and 3.4 for PSN-Bi. However, in the case of Ba-doped PSN, the elastic softening is less pronounced, especially for the low-pressure phase and the $F(f)$ minimum appears to be smeared out over a pressure range 3.5–4.3 GPa, rather than being sharp and well defined at a certain pressure point as for pure and Bi-doped PSN. The same behavior has been observed for Ba-doped PST,[20] which shows an even broader plateaulike minimum of $F(f)$ due to the higher Ba content. Thus the specific shape of the $F(f)$ dependence indicates a diffuse pressure-induced phase transition, which is related to the Ba-induced disturbance of coherent off-centered Pb^{2+} cations. This is also evident in the negligibly small change in the bulk modulus of PSN-Ba near the phase transition [Fig. 1(b)]. In contrast to Ba^{2+}, the incorporation of Bi^{3+} does not smear out the phase transition. The pressure-induced phase transition in PSN-Bi is even more pronounced than that in pure PSN, both with respect to the slope of $K(p)$ below p_c as well as the difference between the low- and high-pressure value of K at the transition point $\Delta K(p_c)$ [Fig. 1(b)]. Considering the structural complexity of relaxors at ambient conditions, namely, PNRs inside a paraelectric matrix, one can assume that the high-pressure structure comprises ferroic nanodomains distributed within a nonferroic matrix. Hence, the values of $\Delta K(p_c)$ and dK/dp suggest that the fraction of spatial regions undergoing a phase transition is largest for PSN-Bi, smaller for PSN, and smallest for PSN-Ba.

At pressures above the phase transition, the diffraction peaks with h, k, l, all even indexed on the $Fm\bar{3}m$ unit cell broaden (Fig. 2). This broadening corresponds to diffraction peak splitting caused by symmetry lowering,[17,29] which cannot be experimentally resolved due to the rather small

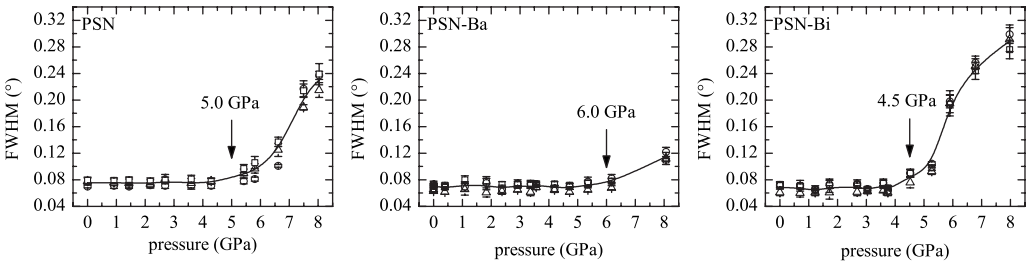

FIG. 2. Pressure evolution of FWHMs for representative reflections of type $h00$ (circles), $h0h$ (squares), and $h0l$ (triangles), $h,l=2n$ (in $Fm\bar{3}m$), obtained by in-house single-crystal XRD experiments for PSN, PSN-Ba, and PSN-Bi. The lines are spline interpolations of the experimental data for guiding the eye. The arrows indicate the approximate pressure values at which FWHMs start increasing.

symmetry-breaking strains. For PST, the broadening is detectable immediately above the critical pressure[17] whereas in the case of pure and doped PSN, the broadening appears at a pressure higher than the transition pressure, most probably due to the smaller fraction of ferroic domains which have therefore less impact on the pseudocubic diffraction peaks. The characteristic pressure at which the FWHMs start increasing can be roughly estimated to 5.0 GPa, 6.0 GPa, and 4.5 GPa for PSN, PSN-Ba and PSN-Bi, respectively. Therefore, the fraction of pressure-induced ferroic domains is larger in PSN-Bi and smaller in PSN-Ba.

Further we compared the HP Raman spectra of PSN-Ba and PSN-Bi (see Fig. 3) with the spectra of pure PSN.[19] A detailed assignment of the observed spectral features is given elsewhere.[20] Due to the relatively low content of Ba and Bi, we have used the same number of replicas for analyzing the spectra of doped PSN as for pure PSN. As can be seen in Fig. 3, Ba- and Bi-doped PSN exhibit the pressure-induced spectral changes which are typical of all Pb-based relaxors studied so far:[15–20] (i) weakening of the Raman signal near 150 cm^{-1} due to the decoupling of off-center Pb and B cations in polar nanoregions, which is a precursor for a phase transition, (ii) a strong suppression of the peak near 260 cm^{-1} reflecting the reduction in off-centered B-cation displacements, and (iii) an enhancement of the Raman scattering near 350 cm^{-1} indicating an enlarged coherence length of correlated Pb-O ferroic species.[17] For PSN-Bi, an additional Raman signal near 35 cm^{-1} is observed above 3.1 GPa, associated with a soft mode near the phase transition. Such a soft mode was clearly observed for PST (Ref. 17) but could not be resolved for pure PSN.[19] This indicates that in PSN-Bi, the fraction of ferroic domains developed at HP is larger than the ferroic domain fraction in PSN, which is in full agreement with the XRD data. A soft mode could not be resolved for PSN-Ba but the kink in the pressure evolution of the wave number ω and the maximum of FWHM of the Pb-localized mode near 50 cm^{-1} (see the inset on left in Fig. 3) mirrors the structural transformations occurring near 4.0

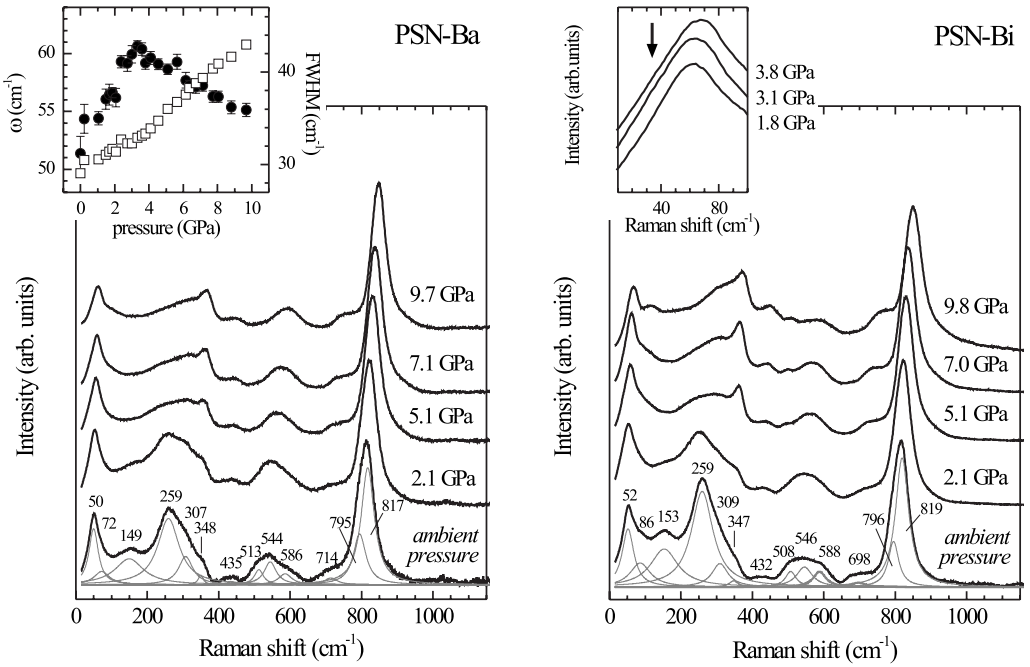

FIG. 3. Raman scattering of PSN-Ba and PSN-Bi at selected pressure points. The inset on left shows the pressure evolution of the wave number (open squares) and FWHM (filled circles) of the Raman peak near 50 cm^{-1}, arising from the Raman-active Pb-localized mode. The inset on right shows on an enlarged scale the appearance of additional Raman scattering near 35 cm^{-1} above 3.1 GPa.

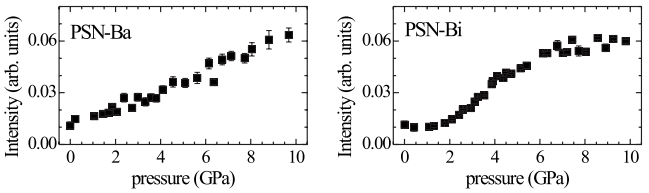

FIG. 4. Pressure dependence of the integrated Raman intensity near 350 cm^{-1} for PSN-Ba and PSN-Bi.

GPa. In the case of pure PSN, the $\omega(p)$ dependence has a pronounced minimum,[19] which reveals a stronger softening of the structure when approaching the phase transition for PSN as compared to PSN-Ba, which is also in accordance with the volume compressibility data.

The pressure evolution of the Raman scattering near 350 cm^{-1}, originating from Pb-O bond-stretching modes in ferroic regions, also underlines the different effects of Ba and Bi on the pressure-induced structural transformations in PSN (see Fig. 4). PSN-Ba shows a gradual increase in intensity with pressure, without any peculiarity whereas for PSN-Bi, the intensity variation exhibits an inflection near p_c =3.4 GPa, thus better revealing the occurrence of a phase transition. Apparently, the dilution of Pb^{2+} with Ba^{2+} disturbs the ordering processes in the *A*-O system and thus smears out the phase transition while the substitution of Bi^{3+} for Pb^{2+} favors the ferroic atomic clustering in the *A*-O system, regardless of the charge imbalance that has been introduced by *A*-site doping. However, Ba and Bi have similar effect on the Raman scattering near 260 cm^{-1} that originates from off-centered *B* cations (see Fig. 5). Pure PSN is characterized by a considerable, abrupt decrease in the intensity of this mode near p_c=4.1 GPa, as well as a well pronounced maximum of FWHM vs pressure and a minimum of $\omega(p)$. These spectral features indicate a decrease in the off-centered displacements of *B* cations near the phase transition. Further spectral changes reveal that near 6 GPa, the system reaches a saturation of suppressed *B*-cation off-centered shifts.[19] Similarly to PSN, PSN-Ba, and PSN-Bi have a minimum of $\omega(p)$ near 4 GPa which however is considerably broader for the two doped compounds. In addition, up to ~3.5 GPa, the peak width increases and then remains nearly constant, without showing a maximum. At the same time, the intensity gradually decreases at pressures above 3.5 GPa, without reaching a saturation; this is especially pronounced for PSN-Bi. The trends in the FWHMs and integrated intensities indicate that both Ba^{2+} and Bi^{3+} impede the movement of *B* cations toward the octahedral centers. In the case of PSN-Ba, this is most probably due to the local elastic fields in the vicinity of Ba^{2+} cations on the *A* site while in the case of PSN-Bi, the effect should be related to local electric fields associated with Bi^{3+} on the *A* site.

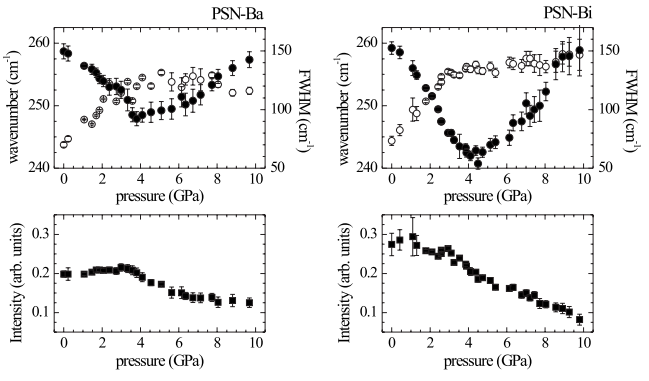

FIG. 5. Pressure dependence of the wave number (filled circles), FWHM (open circles), and integrated intensity (filled squares) of the Raman scattering near 260 cm^{-1} for PSN-Ba and PSN-Bi.

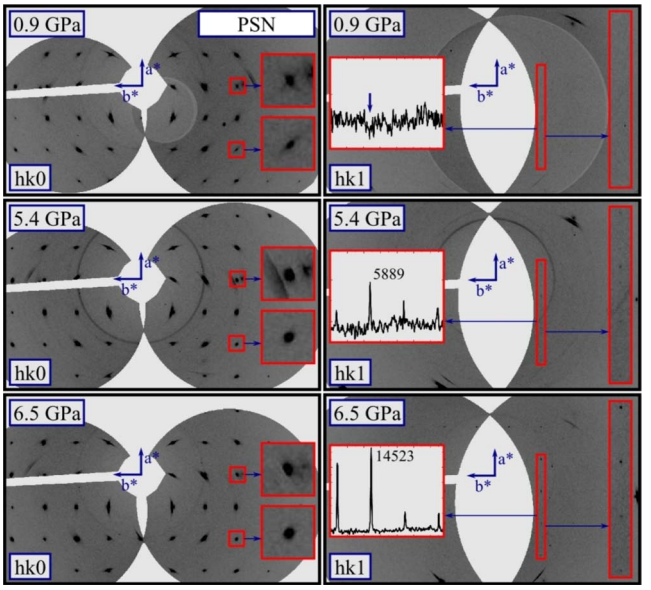

FIG. 6. (Color online) Reciprocal space layers of PSN at three representative pressures. Line profiles are along [*h*31] (in $Fm\bar{3}m$).

Hence, Raman spectroscopic data show that Ba^{2+} and Bi^{3+} have a different impact on the phonons in the lowest-energy range that are dominated by Pb vibrations and on the O-localized mode near 350 cm^{-1} related to Pb-O bond stretching. However, they have quite similar effects on the *B*-localized mode near 260 cm^{-1}. Thus, the combined analysis of the pressure dependence of the unit-cell volume and Raman scattering of pure, Ba- and Bi-doped PSN shows that the high-pressure state comprises ferroically ordered *A*-O structural species and does not involve ferroic arrangements of the *B* cations.

To gain more insight into the high-pressure state, we have also conducted synchrotron single-crystal XRD. Figure 6 shows reciprocal space layers reconstructed from the raw diffraction images of PSN at three representative pressure values. The (*hkl*) layers, with $l=2n$ (in $Fm\bar{3}m$) show the pressure evolution of the x-ray diffuse scattering originating from polar nanoclusters.[30,31] For all Pb-based perovskite-type relaxors studied up to now, the diffuse x-ray scattering is along the $\langle 110\rangle^*$ directions of the reciprocal space and is strongly suppressed at HP.[13,15–17] As can be seen in Figs. 6–8, this is also typical of PSN, PSN-Ba, and PSN-Bi, respectively. The weakening of the x-ray diffuse scattering at HP indicates that the polar nanoregions comprising off-centered Pb and *B*-cation displacements present at ambient pressure[30,32] are altered by pressure. The x-ray scattering data alone do not distinguish whether such a process of

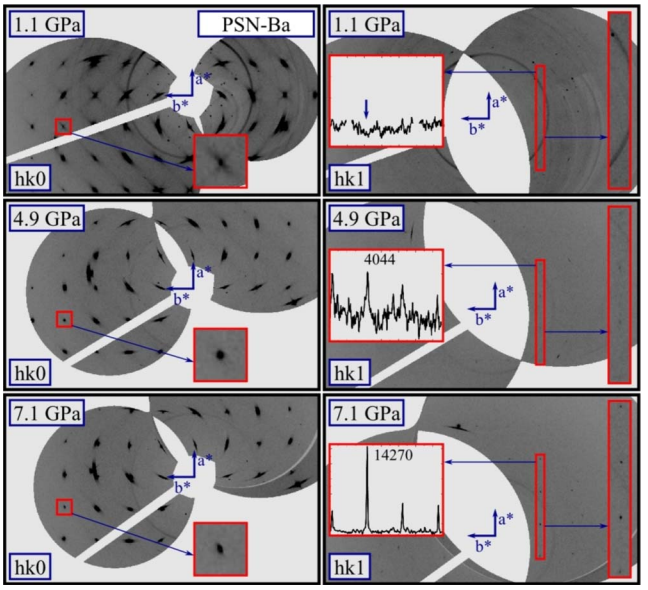

FIG. 7. (Color online) Reciprocal space layers of PSN-Ba at three representative pressures. Line profiles are along [*h*31] (in $Fm\bar{3}m$).

transformation occurs by the development of long-range ordering of cation displacements and/or by the suppression of the magnitudes of the displacements. The Raman-scattering data clearly show that pressure leads to a decrease in the off-centered displacements of the *B* cations above the transition. Recent structural refinements of HP XRD and neutron-diffraction data on pure and Ba-doped PST indicate that the magnitude of Pb off-centered displacements is also reduced by pressure above the transition.[29] It therefore appears that a decrease in the intensity of the diffuse scattering indicates *both* the development of longer-range ferroic order of the

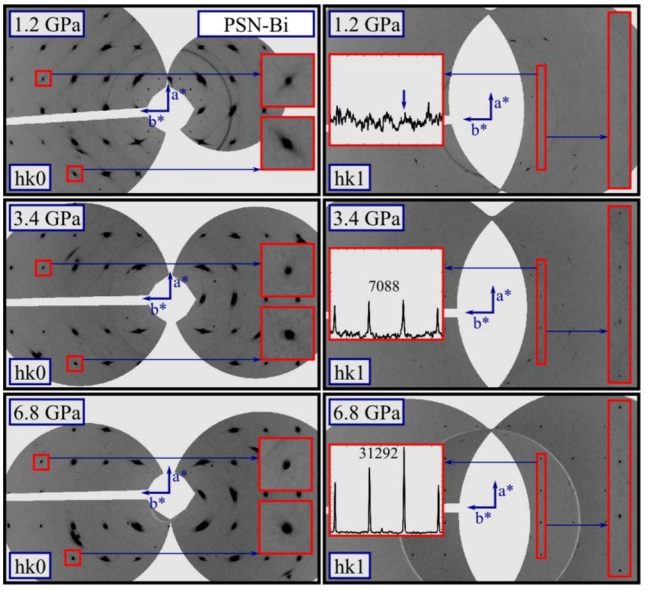

FIG. 8. (Color online) Reciprocal space layers of PSN-Bi at three representative pressures. Line profiles are along [*h*31] (in $Fm\bar{3}m$).

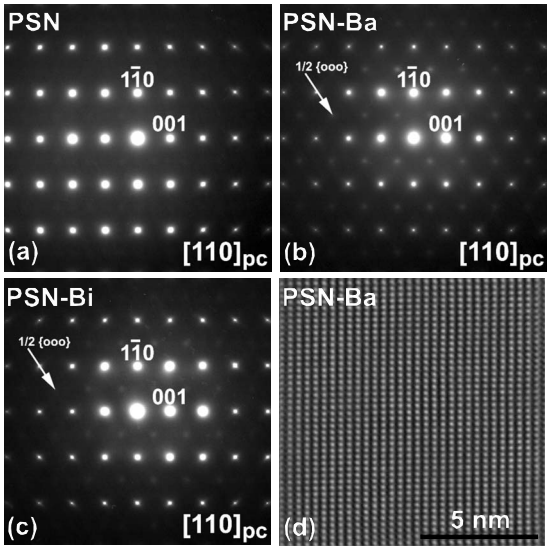

FIG. 9. TEM images along the primitive cubic [110] direction. (a) SAED of PSN, showing extremely weak 1/2{ooo} superlattice reflections. (b) SAED of PSN-Ba; 1/2{ooo} superstructure reflections are visible, marked with an arrow. (c) SAED of PSN-Bi, also showing more intense 1/2{ooo} superlattice reflections as compared to PSN. (d) HRTEM image along $[110]_{pc}$ direction; an inverse Fourier-transformed HRTEM image was overlayed with 50% opacity on the original HRTEM image.

cation displacements, followed by a decrease in the magnitude of those displacements with further pressure increase. For all three PSN compounds, the x-ray diffuse scattering significantly decreases in intensity above the corresponding critical pressure (Figs. 6–8), indicating that the transitions are also related to the development of pressure-induced ferroic order.

For all three compounds, pressure-induced diffraction peaks in the (*hk*1) layers are observed above p_c and their intensity increases with pressure (see Fig. 6–8). At ambient pressure, the presence of Bragg reflections with *h*, *k*, *l*, all odd, is indicative of chemically 1:1 *B*-site long-range ordered regions.[33,34] For all three compounds studied, no odd-odd-odd diffraction peaks are observed in the DAC at low pressures. Using the same beamline to conduct synchrotron single-crystal XRD in air (not in a DAC), long-range CBO was detected for PSN via weak reflections in the (*hk*1) layer but not in PSN-Ba and PSN-Bi.[21] The absence of the weak odd-odd-odd reflections for PSN measured in the DAC is due to attenuation of the beam by the diamond anvils and is indicative of a very low degree of long-range CBO in PSN, comparable with that in Ba- and Bi-doped PSN. To verify the abundance and the size of CBO regions we have additionally performed TEM experiments (see Fig. 9). The SAED patterns of all three compounds reveal a low degree of chemical *B*-site order even on a local scale. Pure PSN sporadically exhibits odd-odd-odd reflections with extremely weak intensities, which confirms that CBO regions are not a characteristic feature of this single-crystal sample. The odd-odd-odd Bragg reflections are better resolved in the SAED pattern of PSN-Bi and are strongest for PSN-Ba. Figure 9 also depicts the HRTEM image of PSN-Ba; the HRTEM images of PSN;

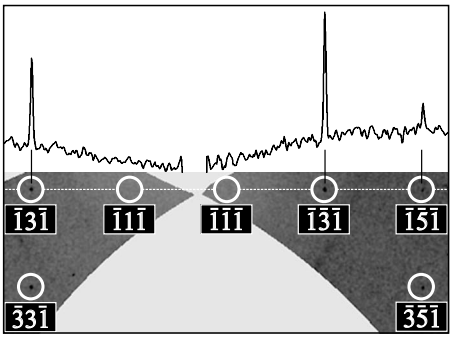

FIG. 10. $(hk\bar{1})$ layer of {110}-cut PSN at 5.4 GPa and line profile along $[\bar{1}k\bar{1}]$ (in $Fm\bar{3}m$).

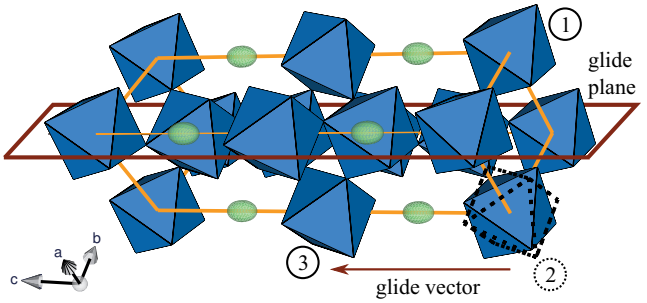

FIG. 11. (Color) Schematic view of the high-pressure structure of Pb-based perovskite-type relaxors in the case of complete chemical *B*-site disorder. The BO_6 octahedra are given in blue. The two-step glide-plane symmetry transformation is representatively shown for octahedron ①: reflection on the glide plane yields the intermediate octahedron ② (dashed lines), which is subsequently translated by the glide vector to octahedron ③. The Pb atoms are shown by green ellipsoids; the ellipsoidal elongation represents the anisotropy in the atomic displacement parameters (Ref. 29). The yellow line represents the unit cell. The octahedral tilt configuration is the same in the case of chemical *B*-site ordering but strictly speaking, the glide-plane symmetry is violated and should be considered as pseudosymmetry. The figure was prepared using the VESTA software package (Ref. 36).

and PSN-Bi single crystals resemble that of PSN-Ba. A clear indication for local ordering could not be verified by HR-TEM analysis but the absence of abundant large-size CBO regions is apparent for all three compounds.

The narrow width of Bragg reflections with *h*, *k*, *l*, all odd, observed at $p > p_c$ points to long correlation lengths of coherently scattering domains. As the chemical order cannot change with pressure, the additional odd-odd-odd Bragg reflections must originate from the pressure-induced structural transformations. Three distinct processes can contribute to these diffraction peaks: (i) an out-of-phase tilting of the BO_6 octahedra which might well be observable by XRD for the given exposure times; pressure-induced odd-odd-odd XRD peaks have been also reported for $PbMg_{1/3}Nb_{2/3}O_3$ (Ref. 13) and $PbZn_{1/3}Nb_{2/3}O_3$,[16] and assumed to arise from long-range octahedral tilting;[16] (ii) an antiparallel ordering of off-centered Pb cations, as already suggested in the case of PST;[17] and (iii) a decrease in uncoupled polar *B*-cation displacements as revealed by Raman spectroscopy, which would facilitate the observation of spatial regions with chemical *B*-site ordering. Structure-factor calculations show that the suppression of incoherent off-center displacements of *B*-site cations cannot give rise to the observed XRD intensity. Besides, TEM data clearly show the absence of abundant *B*-site long-range ordered regions. Thus, the pressure-induced diffraction peaks can result from either ferroic order of Pb displacements and/or development of coherent tilting of the BO_6 octahedral system.

Synchrotron XRD experiments performed on a {110}-cut single crystal of PSN clearly shows the absence of (*hhh*), $h=n$, reflections (see Fig. 10) whereas other odd-odd-odd Bragg reflections are observed. In the complete absence of any CBO, this systematic absence would indicate the presence of glide-plane symmetry due to antiphase tilting of the octahedra.[35] Given we cannot completely exclude either the presence of low CBO in these samples or some patterns of *A*-cation displacements that would violate this glide symmetry, we can only state that this systematic absence strongly indicates that the ferroic distortion results in a glide-plane pseudosymmetry of the average structure (a possible rhombohedral structure is shown in Fig. 11). It therefore suggests that a combination of antiphase octahedral tilting and locally ordered Pb displacements is a characteristic feature of the HP phase of Pb-based relaxors. The pressure-induced long-range octahedral tilt order results in more distorted PbO_{12} polyhedra, which explains the strong intensity increase in the Raman peak near 350 cm^{-1} arising from the bond-stretching vibrations in correlated ferroic Pb-O species. The much stronger diffraction intensities of the additional odd-odd-odd peaks for PSN-Bi, as compared to pure and Ba-doped PSN, unambiguously reveal that the incorporation of three-valent cations with LPE into the host system of two-valent cations with LPE enhances the distortion to lower symmetry. Structure refinements of HP neutron powder-diffraction data and synchrotron XRD data from PST are currently in progress to determine the actual atomic configuration in Pb-based relaxors.

IV. CONCLUSIONS

The relaxor-ferroelectric PSN exhibits a pressure-induced phase transition at 4.1 GPa and the high-pressure phase has glide-plane pseudosymmetry consistent with antiphase octahedral tilts and antiparallel Pb displacements. A moderate level of *A*-site doping with Ba (Ba/Pb+Ba=0.07) and Bi (Bi/Pb+Bi=0.02) slightly decreases the critical pressure. However, the change in the critical pressure does not correlate with the degree of doping, revealing the complex effect of the two dopants on the atomic arrangements in Pb-based perovskite type relaxors, due to the difference between the electronic structures of Ba and Bi. The replacement of Pb^{2+} in the *A* sites by isovalent cations (Ba^{2+}) having a larger ionic radius and no stereochemically active lone-pair electrons smears the pressure-induced phase transition due to the introduction of local elastic fields in the structure. By contrast, the replacement of Pb^{2+} in the *A* sites by aliovalent cations (Bi^{3+}) having nearly the same ionic radius and active lone-pair electrons enlarges the fraction of spatial regions

with a pressure-induced ferroic distortion, resulting in a more pronounced phase transition of the average structure. The distinctive effect of the two types of *A*-site dopants on the structural changes under pressure is totally consistent with the corresponding effect on the temperature-driven structural transformations in Pb-based relaxors.[21] Apparently, the local electric fields associated with Bi^{3+} incorporated on the *A* site induces additional nucleation of noncubic structural species involving cation shifts. At the same time, the preserved lone-pair order and absence of strong local elastic fields favors long-range ferroic order, thus enhancing the overall ferroicity on pressure increase as well as on temperature decrease. However, cooling favors polar cation shifts whereas pressure seems to favor significant octahedral tilting. The results cannot unambiguously reveal if the high-pressure ferroic state of Pb-based relaxors is polar, as the low-temperature state, or nonpolar.

ACKNOWLEDGMENTS

Financial support by the Deutsche Forschungsgemeinschaft (MI 1127/2, GK 611, INST 152/485-1 FUGG, WI 1232/25-1, and SPP1236 central facility), the National Science Foundation (Grant no. EAR-0738692), and the Bulgarian Ministry Science and Education (BY-X-308) is acknowledged. We would like to thank Mathias Müller, Universität Darmstadt, for TEM sample preparation and Pierre Toledano, University of Picardie, for fruitful discussions.

*bernd.maier@mineralogie.uni-hamburg.de
†boriana.mihailova@uni-hamburg.de

[1] A. A. Bokov and Z.-G. Ye, J. Mater. Sci. **41**, 31 (2006).
[2] K. Hirota, S. Wakimoto, and D. E. Cox, J. Phys. Soc. Jpn. **75**, 111006 (2006).
[3] A. Gruverman and A. Kholkin, Rep. Prog. Phys. **69**, 2443 (2006).
[4] G. A. Samara, J. Phys.: Condens. Matter **15**, R367 (2003).
[5] I.-W. Chen, P. Li, and Y. Wang, J. Phys. Chem. Solids **57**, 1525 (1996).
[6] L. A. Bursill, P. JuLin, Q. Hua, and N. Setter, Physica B **205**, 305 (1995).
[7] R. Blinc, A. Gregorovic, B. Zalar, R. Pirc, V. V. Laguta, and M. D. Glinchuk, Phys. Rev. B **63**, 024104 (2000).
[8] A. S. Bhalla, R. Guo, and R. Roy, Mater. Res. Innovations **4**, 3 (2000).
[9] B. P. Burton, E. Cockayne, S. Tinte, and U. V. Waghmare, Phase Transitions **79**, 91 (2006).
[10] C. Malibert, B. Dkhil, J. M. Kiat, D. Durand, J. F. Bérar, and A. Spasojevic-de Biré, J. Phys.: Condens. Matter **9**, 7485 (1997).
[11] V. Marinova, B. Mihailova, T. Malcherek, C. Paulmann, C. Lengyel, L. Kovacs, M. Veleva, M. Gospodinov, B. Güttler, R. Stosch, and U. Bismayer, J. Phys.: Condens. Matter **18**, L385 (2006).
[12] G. A. Samara and E. L. Venturini, Phase Transitions **79**, 21 (2006).
[13] B. Chaabane, J. Kreisel, B. Dkhil, P. Bouvier, and M. Mezouar, Phys. Rev. Lett. **90**, 257601 (2003).
[14] J. Kreisel, P. Bouvier, B. Dkhil, P. A. Thomas, A. M. Glazer, T. R. Welberry, B. Chaabane, and M. Mezouar, Phys. Rev. B **68**, 014113 (2003).
[15] M. Ahart, R. E. Cohen, V. Struzhkin, E. Gregoryanz, D. Rytz, S. A. Prosandeev, H.-K. Mao, and R. J. Hemley, Phys. Rev. B **71**, 144102 (2005).
[16] P. E. Janolin, B. Dkhil, P. Bouvier, J. Kreisel, and P. A. Thomas, Phys. Rev. B **73**, 094128 (2006).
[17] B. Mihailova *et al.*, Phys. Rev. Lett. **101**, 017602 (2008).
[18] B. Chaabane, J. Kreisel, P. Bouvier, G. Lucazeau, and B. Dkhil, Phys. Rev. B **70**, 134114 (2004).
[19] A.-M. Welsch, B. Mihailova, M. Gospodinov, R. Stosch, B. Güttler, and U. Bismayer, J. Phys.: Condens. Matter **21**, 235901 (2009).
[20] A.-M. Welsch *et al.*, Phys. Rev. B **80**, 104118 (2009).
[21] B. J. Maier, B. Mihailova, C. Paulmann, J. Ihringer, M. Gospodinov, R. Stosch, B. Güttler, and U. Bismayer, Phys. Rev. B **79**, 224108 (2009).
[22] R. Miletich, D. R. Allan, and W. F. Kuhs, in *High-Pressure and High-Temperature Crystal Chemistry*, Reviews in Mineralogy and Geochemistry, Vol. 41, edited by R. M. Hazen and R. T. Downs, (Mineralogical Society of America, 2000), WA, pp. 445.
[23] R. J. Angel, D. R. Allan, R. Miletich, and L. W. Finger, J. Appl. Crystallogr. **30**, 461 (1997).
[24] H. King and L. W. Finger, J. Appl. Crystallogr. **12**, 374 (1979).
[25] R. J. Angel, R. T. Downs, and L. W. Finger, in *High-pressure and High-temperature Crystal Chemistry*, Reviews in Mineralogy and Geochemistry Vol. 41, edited by R. M. Hazen and R. T. Downs (Mineralogical Society of America, 2000), pp. 559.
[26] R. Boehler, Rev. Sci. Instrum. **77**, 115103 (2006).
[27] R. G. Munro, G. J. Piermarini, S. Block, and W. B. Holzapfel, J. Appl. Phys. **57**, 165 (1985).
[28] R. J. Angel, M. Bujak, J. Zhao, G. D. Gatta, and S. D. Jacobsen, J. Appl. Crystallogr. **40**, 26 (2007).
[29] B. J. Maier, R. J. Angel, W. G. Marshall, B. Mihailova, C. Paulmann, J. Engel, M. Gospodinov, A.-M. Welsch, and U. Bismayer, Acta Crystallogr., Sect. B: Struct. Sci. **66**, 280 (2010).
[30] T. R. Welberry and D. J. Goossens, J. Appl. Crystallogr. **41**, 606 (2008).
[31] G. Xu, Z. Zhong, Y. Bing, Z.-G. Ye, and G. Shirane, Nature (London) **5**, 134 (2006).
[32] M. Paściak, M. Wolcyrz, and A. Pietraszko, Phys. Rev. B **76**, 014117 (2007).
[33] N. Setter and L. E. Cross, J. Appl. Phys. **51**, 4356 (1980).
[34] C. G. F. Stenger and A. J. Burggraaf, Phys. Status Solidi A **61**, 275 (1980).
[35] C. J. Howard and H. T. Stokes, Acta Crystallogr., Sect. A: Found. Crystallogr. **61**, 93 (2004).
[36] K. Momma and F. Izumi, J. Appl. Crystallogr. **41**, 653 (2008).